Co-rich magnetic amorphous films and their application in magnetoelectronics

Y. Luo, M. Esseling, A. Käufler, and K. Samwer
I. Physikalisches Institut, Universität Göttingen, Friedrich-Hund Platz 1, D-37077 Göttingen, Germany

T. Dimopoulos, G. Gieres, M. Vieth, M. Rührig, and J. Wecker
Siemens AG, Corporate Technology, Paul-Gossen-Str. 100, D-91052 Erlangen, Germany

C. Rudolf, T. Niermann, and M. Seibt
IV. Physikalisches Institut, Universität Göttingen, Friedrich-Hund Platz 1, D-37077 Göttingen, Germany
(Received 12 October 2004; published 13 July 2005)

Three kinds of Co-rich magnetic amorphous films of CoFeB, CoFeNiSiB, and CoFeHfO were prepared by magnetron sputtering and applied as soft ferromagnetic (FM) electrodes in tunneling magnetoresistance (TMR) devices. Initial results exhibit a large room-temperature TMR effect of approximately 50%. The high effect can be attributed to interfacial coherence between the amorphous barrier-electrode layers and, accordingly, suggests a high local spin polarization possibly associated with strong nearest-neighbor spin correlations of the magnetic atoms. The magnetotransport behavior may be governed by details of the local spin environment in magnetic amorphous electrodes due to their short electron mean-free path (~3–5 Å). The annealing effect on TMR was found to be more pronounced due to the atomic cooperative structural relaxation and more thermally stable compared with the polycrystalline electrode junctions. Additionally, the use of the magnetic oxide electrode CoFeHfO has shown that the relevant FM electrode-barrier interface becomes insensitive to the oxygen, which simplifies the oxidation process used for the oxide barrier fabrication.

DOI: 10.1103/PhysRevB.72.014426 PACS number(s): 85.30.Hi, 85.75.−d, 72.25.−b, 75.50.Kj

I. INTRODUCTION

With the progress in magnetoelectronics, the tunneling magnetoresistance (TMR) effect in magnetic tunneling junctions (MTJs) is widely studied nowadays. A MTJ device mainly consists of two ferromagnetic layers, F_1 and F_2, as tunneling electrodes separated by an oxide insulating layer as an electrical barrier. One electrode is hard magnetic with a coercivity of H_{c1} or it is exchange biased by a natural antiferromagnet. The other electrode, designated as the "detection layer," is comprised of a soft ferromagnet with H_{c2} smaller than H_{c1}. In this case, the relative orientation of the magnetic moments in the two electrodes can be changed from parallel to antiparallel by switching the detection layer using an external magnetic field. Associated with the spin-polarized electronic structure, TMR arises from varied tunnel probabilities of the majority and minority electrons for the two magnetization configurations. The tunnel resistance R_P for the parallel alignment is normally lower than R_{AP} for the antiparallel and the ratio of $\Delta R/R_P$ gives the magnitude of the TMR effect. The Jullière model[1] connects the magnitude of TMR and the spin polarization P, i.e., TMR $=2P_1P_2/(1-P_1P_2)$ and guides developing of MTJs with high P ferromagnets including half-metallic ferromagnets, such as CrO_2 (Ref. 2) and manganite oxides.[3–5] Also, much effort has been made in the past for optimizing the tunneling barrier and its interfacial state.[6–9] In the case of metal-oxide systems, the interfacial state is particularly sensitive to the oxidation procedure used for the barrier fabrication. Taking magnetic oxide electrodes is a good choice for simplifying the oxidation process regarding junction interfaces. Moreover, the structural mismatch between the barrier and electrode layers could be the origin of extra layer roughness and leads to an increase in spin-independent scattering of the charge carriers. Interfacial coherent systems, such as epitaxially grown systems of α-Al_2O_3/Fe (Ref. 10) and MgO/Fe (Ref. 11) were designed recently, showing a high spin polarization and a large TMR effect. Otherwise, the mostly used tunneling barrier Al_2O_3 is prepared in a nonequilibrium condition and shows an amorphous structure. As a matter of course, noncrystalline ferromagnets become candidates for junction electrodes to match the insulating layer microstructure.[12] Because of structural isotropy on a long-range scale, amorphous films should be growing exceptionally smooth.

In this paper, we report on structural and magnetotunneling measurements for MTJs containing soft magnetic noncrystalline films of $Co_{64}Fe_5Ni_5Si_{13}B_{13}$, $Co_{60}Fe_{20}B_{20}$, or $Co_{55}Fe_{25}Hf_{20}$ oxide, respectively, as the detection layer. The three kinds of alloys are quasi-binary, i.e., $(CoFeNi)_{74}(SiB)_{26}$, $(CoFe)_{80}B_{20}$, and $(CoFe)_{80}Hf_{20}$, have a Co content of 64 at. %, 60 at. %, and 55 at. %, respectively, and hence they are Co rich.

The first and the second alloys belong to transition metal-metalloid-type metallic glasses, stemming actually from the parent alloy of $Co_{80}B_{20}$, where 20 at. % metalloid was chosen based on the glass formation range which is centered around a deep eutectic at approximately 20% metalloid. Associated with the atomic size effect, the glass forming ability is enhanced intentionally by adding Fe, Ni, or—the second metalloid—Si. Generally, for a lack of grain boundaries for the pinning of domain walls, these metallic glasses behave as a very soft magnetic with rather small H_c (about 0.1–1 Oe). As is indicated by thermomagnetic studies,[13] the Curie temperature of these glasses lies between 400 and 500 °C, slightly above the crystallization temperature. Because of the

TABLE I. Structure of MTJs studied, involving the junction size, pinning of electrodes, oxidation of the Al_2O_3 barrier, and the TMR ratios measured before and after annealing.

MTJs	$F_1//F_2$ thickness	Oxid. of Al_2O_3 thickness	Pinning	Junction size patterned by	TMR @=annealed
J_1	CoFe//CoFeB	Plasma	IrMn/AAF	20×20 μm^2	—
	2.8 nm//4 nm	2 nm	$CoFe/Ru/F_1$	lithography	50% @ at 270 °C
J_{2a}	Co//CoFeNiSiB	Plasma	AAF	10×10 μm^2	12% as prepared
	1.5 nm//6 nm	2 nm	$Co/Cu/F_1$	lithography	23% @ at 230 °C
J_{2b}	CoFe//CoFeNiSiB	Plasma	AAF	10×10 μm^2	10% as prepared
	1.5 nm//6 nm	2 nm	$CoFe/Ru/F_1$	lithography	24% @ at 150 °C
J_{3a}	CoFeHfO//CoFe	Reactive sputter	Co	50×50 μm^2	11% at 200 K
	10 nm//2 nm	1.5 nm		shadow masks	—
J_{3b}	CoFeHfO//CoFeNiSiB	Reactive sputter	Co	50×50 μm^2	—
	10 nm//4 nm	1.0 nm		shadow masks	28% @ at 250 °C

loss of periodicity, the electrical transport behaviors can no longer be described by the Bloch wave and the Boltzmann transport equation may not be valid. The electrical resistivity, which is dominated by disorder scattering, was found to be two or three times larger than that measured for the crystallized films and revealed a small negative temperature coefficient below the Curie temperature. The short electron mean-free path of the order of interatomic distances implies that the electrical transport behavior appears to probe the details of the local environment in the films preferentially over other long-range properties. Moreover, as is well established, the Co-based glasses are strong ferromagnets with minority spin holes only,[14,15] suggesting an exceptionally high spin polarization. The substitution of the other 3*d*-transition metals, Fe and Ni, increases the magnetic moment and decreases the magnetostriction ($\sim10^{-6}$).[14] Additionally, as pointed out in Ref. 16, the coexistence of two or more different kinds of transition metals is more effective in developing a strong uniaxial magnetic anisotropy which is essential for MTJ applications. The third kind of the alloy, $(CoFe)_{80}Hf_{20}$, innovates actually in the type of metallic glasses consisting of one or more 3*d*-transition metals and a group-IVB metal (Zr, Hf, or Ti), such as alloys of $(CoFe)Zr_{9-16}$ (Ref. 17) which also showed potentially useful soft magnetic properties. Dissimilarly, the films used here were prepared under a reactive gas condition. Thus, they are oxidic (denoted below as CoFeHfO) and expected to be noncrystalline. As mentioned above, an oxide electrode brings additional advantages to MTJs, i.e., the relevant interfaces should become insensitive to oxygen. In this case, the oxidation procedures used afterward for oxide barrier fabrications become much more simplified.

II. EXPERIMENTAL DETAILS

Magnetic amorphous films including relevant MTJs were magnetron sputtered from alloy targets of $(CoFe)_{80}B_{20}$, $(CoFeNi)_{74}(SiB)_{26}$, and $(CoFe)_{80}Hf_{20}$ onto thermally oxidized Si(100) substrates in multigun systems with a base pressure of $\sim10^{-8}$ mbar and a working pressure Ar of about $\sim10^{-3}$ mbar. A magnetic field was applied during the film deposition to induce uniaxial magnetic anisotropy, arising from pair ordering of the magnetic atoms.[16] The chemical stoichiometry of the prepared films has been checked by electron microprobe and is in accordance with that of the targets. Additionally, the reactive sputtering was performed in a gas mixture of argon and oxygen for the fabrication of CoFeHfO oxide layers. The samples were characterized by structural and magnetic measurements, including x-ray diffraction, Kerr microscopy, magneto-optical Kerr effect (MOKE), and high-resolution transmission electron microscopy (HRTEM).

Table I gives the main structures ($F_1/Al_2O_3/F_2$) of the MTJs referred to as J_1, J_2, and J_3, respectively, with the forementioned three different amorphous films as electrode layers and involves the junction size and oxidation conditions of the Al_2O_3 barrier. As hard electrode, J_1 uses an artificial antiferromagnet (AAF) of CoFe/Ru/CoFe exchange biased by IrMn, while J_{2a} and J_{2a} use a stand-alone AAF. The construction of J_3 is relatively simple, where the junction trilayer was covered by a Co layer for pinning the upper electrode.

Magnetotunneling measurements were performed at room temperature for the junctions (except J_{3a}) with a size of 20×20 μm^2, 10×10 μm^2 (J_1,J_2) patterned by optical lithography, and 50×50 μm^2 (J_3) prepared by shadow masks, respectively. The magnetic field was applied in plane during the measurements.

The annealing of the MTJs was carried out with an external magnetic field applied along the easy axis of the detection electrode. The field annealing is necessary to set the unidirectional exchange bias. It also determines the easy axis of the soft layer.

III. RESULTS AND DISCUSSION

In-plane MOKE loops were measured for single glassy films of CoFeNiSiB and CoFeHfO and plotted in Figs. 1(a) and 1(b), respectively. Soft magnetic properties with a well-defined uniaxial magnetic anisotropy can be identified by rectangular loops along the easy axis, showing a remanence close to the saturation magnetization and a small coercivity of about 2–3 Oe. The loops along the hard axis display an

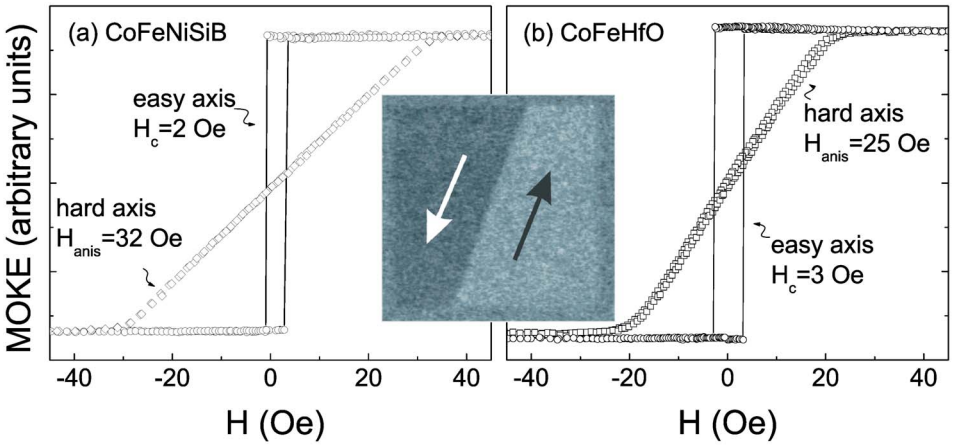

FIG. 1. (Color online) In-plane MOKE loops measured for soft magnetic amorphous films of CoFeNiSiB (a) and CoFeHfO (b), showing well-defined uniaxial magnetic anisotropy associated with sharp 180°-type magnetic domains (inset).

anisotropic field H_{anis} of ~25–32 Oe. The coercive field can be effectively minimized down to about 1 Oe by applying a buffer layer of Ta.[13] The inset of Fig. 1 demonstrates the corresponding magnetic microstructure obtained by Kerr microscopy for the CoFeNiSiB film (6 nm) which was demagnetized and patterned in 100×100 μm^2. As is typical for magnetic metallic glasses, one observes sharp 180°-type domains with the magnetic moments antialigned along the easy axis. The sharp 180° wall mirrors the character of the strong uniaxial magnetic anisotropy in regard to the hysteresis behavior.

Cross-section HRTEM images obtained for J_1 and J_2 are illustrated in Figs. 2(a) and 2(b), respectively. The high-quality layer stack can be verified. The light stripe indicates the barrier layer of Al_2O_3 which is continuous in a quite large scale. Both the top electrode and the Al_2O_3 barrier reveal a typically noncrystalline microstructure without long-range ordering and thus they are microstructurally matched across the common interface. Furthermore, the electron diffraction was carried out for the electrode layers of CoFeNiSiB and CoFeB. They have similar diffraction patterns [see Fig. 2(c)] with a few halolike diffuse rings only where, as typical character for metallic glasses, the second ring is

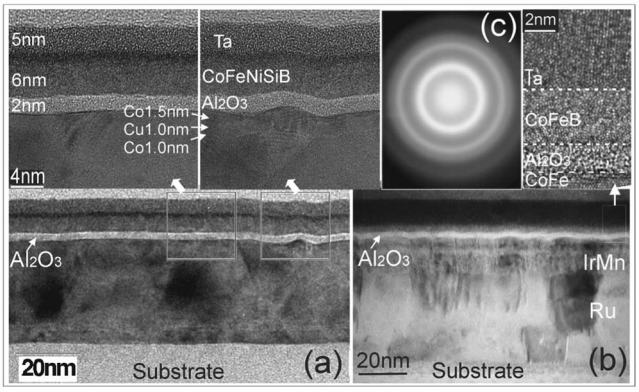

FIG. 2. Cross-section HRTEM images (a) for J_{2a} with CoFeNiSiB and (b) for J_1 with CoFeB as the soft magnetic detection layer, showing a typical noncrystalline microstructure both in the barrier and the upper electrode layers, and thus a matched common interface. (c) Electron diffraction rings obtained from the relevant upper electrode layers.

spilt into two subrings. The result indicates a disordered atomic arrangement but with short-range order. The first diffuse ring has a scattering vector ($q=4\pi/\lambda\cdot\sin\theta$ with the wavelength λ and the diffraction angle θ) of about 3.10 $Å^{-1}$ which corresponds to nearest atomic correlations dominated by Co-Co(Fe). By means of Fourier transforms from the diffraction pattern,[18] the average interatomic distance was found to be 2.53 Å and agrees with the atomic diameters of the magnetic transition elements. The dominated Co -Co(Fe) atomic correlation promotes the pair ordering of the atomic atoms. The nearest-neighbor spin correlations determine magnetic and electrical transport behaviors of the magnetic amorphous films, i.e., strong magnetic anisotropy and high local spin polarization.

Furthermore, as can be followed in Fig. 2 on the other side of the barrier, the HRTEM images reveal a polycrystalline lattice structure within the bottom magnetic electrodes, suggesting that the interface with the barrier layer is structurally incoherent, though it appears to be quite straight due to a small layer roughness [Fig. 2(a)]. At a few positions, the interfaces become more or less undulated, arising evidently from orientation-dependent growth of the polycrystalline layers, but they remain rather correlated.

TMR ratios measured at room temperature for MTJs containing magnetic amorphous electrodes are listed in Table I and the corresponding loops are plotted in Figs. 3–5. The largest TMR value of about 50% was found for J_1 (Ref. 19) and even exceeds the values as far as is known for the MTJs with two polycrystalline magnetic electrodes, such as $CoFe/Al_2O_3/CoFe$ systems.[20] The comparison indicates that the larger magnetotunneling effect observed here can be partly attributed to the microstructural match across the amorphous Al_2O_3/CoFeB interface, where spin-independent scattering and spin transfer of the tunneling electrons may be diminished, compared with incoherent interfaces.[21]

On the other hand, the result implies a high local spin polarization for the magnetic amorphous CoFeB although it contains 20 at. % metalloid. For similar amorphous alloys $(Co_{1-x}Fe_x)_{80}B_{20}$, O'Handley *et al.*[14] introduced a modified split-band model to interpret the changes in magnetic moment M_s and saturation magnetostriction λ with substitution of the second $3d$-transition metal Fe. In this model, the majority-spin $3d^{\uparrow}$ states remain below the Fermi level until M_s reaches a maximum and λ—passing through zero—

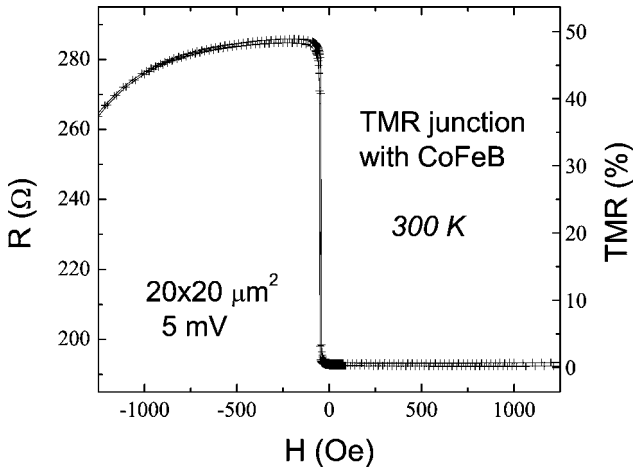

FIG. 3. TMR loop with a ratio of ~50% measured for the tunnel structure $CoFe/Al_2O_3/CoFeB$ (J_1), where the bottom electrode CoFe is pinned by an exchange-bias layer IrMn and the upper electrode CoFeB is noncrystalline with a structural match to the barrier layer of Al_2O_3 which, together with a high local spin polarization for CoFeB, may be responsible for the high TMR effect.

changes its sign. The strongly spin-polarized band structure may be used to understand the large TMR effect found in the CoFeB junction devices. In fact, according to the Jullière model, the spin polarization P_2 for CoFeB can be roughly estimated to be around 0.5 under an assumption of P_1 about 0.40 for the opposite electrode of CoFe. This result predicts a TMR effect of about 70% for MTJs consisting of two CoFeB electrodes.[22]

A relatively lower TMR effect was observed for J_2 with CoFeNiSiB, probably due to higher content of the metalloids (26 at. %) which evidently dilute the total magnetization. Generally, as shown both in the inset of Fig. 4 and in Table I, the as-prepared MTJs display a relatively low TMR effect merely around 10%. However, it goes up drastically after an appropriate annealing. For instance, for the untreated CoNiFeSiB junction J_{2a}, the TMR ratio is about 12%. The effect rises with annealing temperatures and reaches a maximum of about 23% at 230 °C. The annealing-enhanced

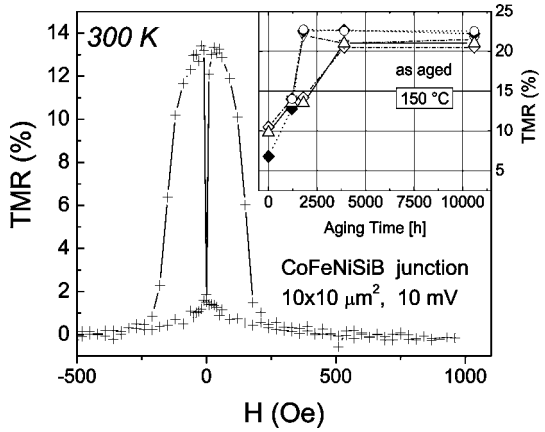

FIG. 4. TMR effects obtained from J_{2a} containing a soft magnetic amorphous film of CoFeNiSiB as the detection electrode. The inset illustrates the annealing effect on TMR values for J_{2b}.

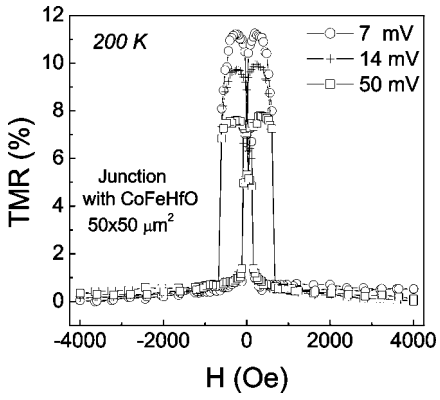

FIG. 5. TMR loops measured at 200 K with different bias voltages for a simple trilayer junction $CoFeHfO/Al_2O_3/CoFe$ (J_{3a}), where the magnetic amorphous oxide of CoFeHfO was considered as the bottom electrode to simplify oxidation procedures used afterward for thin oxide barrier fabrications.

TMR effect can be attributed to the improved microstructure of the junction layers especially in magnetic amorphous layers, where the atomic correlation of Co-Co and the short-range ordering can be enhanced by the induced atomic cooperative structural relaxation[18] due to annealing below the glass temperature. Additionally, it was found that the MTJs studied here are more thermally stable in comparison to those consisting of two CoFe polycrystalline electrodes. After annealing at 400 °C, for instance, the former (J_1) still retains a TMR of about 25%, while for the latter only 5% is left.[21] The higher thermal stability found here reflects a lower atomic configuration energy at the interface between the amorphous barrier-electrode layers.

Figure 5 presents the bias voltage-dependent TMR loops measured for J_{3a} in which the magnetic oxide CoFeHfO was used as the bottom electrode. Its amorphous structure was confirmed before by x-ray scattering experiments, though with a phase separation occurring during the film deposition.[23] The first diffuse peak (not shown here) is thus slightly split, suggesting two interconnected amorphous phases with nearest atomic correlations dominated by Hf-O and Co-Co(Fe), respectively. Nevertheless, the films show excellent soft magnetic properties with strong uniaxial magnetic anisotropy [see Fig. 1(b)]. More importantly, the surface of the CoFeHfO film is insensitive to oxygen, because it has been exposed to ambient atmosphere more than one year before assembling the junctions. For all that, without any additional buffer layers, the simple trilayer junctions exhibit a sufficiently large TMR effect of about 11%. Combined with the amorphous film CoFeNiSiB as the opposite electrode, a TMR effect of about 28% was observed at room temperature in the annealed sample (J_{3b}, see Table I).

IV. CONCLUSION

In summary, in this paper we introduced three kinds of magnetic amorphous films which were prepared by dc-magnetron sputtering and applied as soft magnetic detection electrodes in TMR junction devices. The results indeed

showed a large room-temperature TMR effect of ~50% and can be partly attributed to the structural match across the common interface of the amorphous barrier-electrode layers, where the spin-independent scattering and spin flipping possibilities should be minimized. Otherwise, the high TMR effect suggests a high spin polarization of the amorphous electrode CoFeB, even though it contains 20% metalloid which dilutes the total magnetization. The nearest-neighbor spin correlations of the magnetic atoms may give rise to a locally high spin polarization in accordance with the modified split-band model.[14] Associated with the short electron mean-free path, the magnetotunneling effect could be influenced by the local spin environment in the magnetic amorphous electrode. The annealing effect on TMR was found to be more pronounced therefore due to the structural relaxation of the non-equilibrium amorphous states accompanied by modifications of the local atomic arrangement. Moreover, a relatively higher thermal stability was observed, which mirrors a lower atomic configuration energy at the structurally matched interfaces. Additionally, the attempt on MTJs with the magnetic oxide CoFeHfO offers an alternative for the simplification of the oxidation process in the barrier fabrication.

ACKNOWLEDGMENTS

The authors would like to thank DFG (SA 337/9-1) and BMBF (13N8308) for the support. Also, one of the authors (T.D.) acknowledges support from the European Marie Curie Programme.

[1] M. Jullière, Phys. Lett. **54A**, 225 (1975).
[2] A. Gupta, X. W. Li, and Gang Xiao, Appl. Phys. Lett. **78**, 1894 (2001).
[3] J. Z. Sun, W. J. Gallagher, P. R. Duncombe, L. Krusin-Elbaum, R. A. Altman, A. Gupta, Yu Lu, G. Q. Gong, and Gang Xiao, Appl. Phys. Lett. **69**, 3266 (1996).
[4] M. Bowen, M. Bibes, A. Barthélémy, J.-P. Contour, A. Anane, Y. Lemaître, and A. Fert, Appl. Phys. Lett. **82**, 233 (2003).
[5] Y. Luo, A. Käufler, and K. Samwer, Appl. Phys. Lett. **77**, 1508 (2000).
[6] J. J. Sun, K. Shimazawa, N. Kasahara, K. Sato, T. Kagami, S. Saruki, S. Araki, and M. Matsuzaki, J. Appl. Phys. **89**, 6653 (2001).
[7] J. R. Childress, M. M. Schwickert, R. E. Fontana, M. K. Ho, P. M. Rice, and B. A. Gurney, J. Appl. Phys. **89**, 7353 (2001).
[8] T. Dimopoulos, G. Gieres, S. Colis, J. Wecker, Y. Luo, and K. Samwer, Appl. Phys. Lett. **83**, 3338 (2003).
[9] Y. Luo and K. Samwer, J. Magn. Magn. Mater. **240**, 156 (2002).
[10] Y. S. Dedkov, M. Fonin, U. Rüdiger, and G. Güntherodt, Appl. Phys. Lett. **81**, 2584 (2002).
[11] J. Faure-Vincent, C. Tiusan, E. Jouguelet, F. Canet, M. Sajieddine, C. Bellouard, E. Popova, M. Hehn, F. Montaigne, and A. Schuhl, Appl. Phys. Lett. **82**, 4507 (2003).
[12] A. Käufler, Y. Luo, K. Samwer, G. Gieres, M. Vieth, and J. Wecker, J. Appl. Phys. **91**, 1701 (2002).
[13] A. Käufler, Y. Luo, and K. Samwer, J. Mater. Sci. **39**, 3941 (2004).
[14] R. C. O'Handley and M. O. Sullivan, J. Appl. Phys. **52**, 1841 (1981).
[15] R. C. O'Handley, Solid State Commun. **38**, 703 (1981).
[16] H. Fujimori, *Amorphous Metallic Alloys*, Butterworths Monographs in Materials, edited by F. E. Luborsky (Butterworths, London, 1983), Chap. 16, p. 300.
[17] M. Nose and T. Masumoto, Sci. Rep. Res. Inst. Tohoku Univ. A **A28**, 222 (1980).
[18] Y. Luo, J. Zhao, and S. Huang, Acta Phys. Sin. **31**, 1256 (1983); J. Zhao, Y. Luo, and S. Huang, Chin. Phys. **3**, 547 (1983).
[19] T. Dimopoulos, G. Gieres, J. Wecker, Y. Luo, and K. Samwer, Europhys. Lett. **68**, 706 (2004).
[20] K. I. Lee, J. H. Lee, W. L. Lee, K. H. Shin, Y. B. Sung, J. G. Ha, K. Rhie, and B. C. Lee, J. Appl. Phys. **91**, 7959 (2002).
[21] T. Dimopoulos, G. Gieres, N. Wiese, J. Wecker, and M. D. Sacher, J. Appl. Phys. **96**, 6382 (2004).
[22] D. Wang, C. Nordman, J. Daughton, Z. Qian, and J. Fink, IEEE Trans. Magn. **40**, 2269 (2004).
[23] M. Esseling, Y. Luo, and K. Samwer, Europhys. Lett. **68**, 100 (2004).